



## Valorization of diatomaceous earth as a sustainable eco-coagulant for wastewater treatment: optimization by response surface methodology

Khedidja Benouis <sup>a\*</sup>, Yasmina khane <sup>b</sup>, Tahri Ahmed <sup>c</sup>, Salim Albukhaty <sup>d\*\*</sup>, Shaima R. Banoon <sup>e</sup>

<sup>a</sup>Laboratory of Process Engineering, Materials and Environment, faculty of Technology, University of Djillali Liabes, PO Box 89, Sidi Bel Abbes 22000, Algeria.

<sup>b</sup>Laboratory of Applied Chemistry, ACTR Univ Ain Temouchent, PO Box 284, Ain Temouchent 46000 – Algeria. and, Université de Ghardaia, B.P 455, Ghardaia, Algeria

<sup>c</sup>Unité de Recherche en Energie Renouvelable en Milieu Saharien, URERMs, Centre de Développement des Energies Renouvelables, CDER, Adrar, Algeria.

<sup>d</sup>Department of Chemistry, College of Science University of Misan, Maysan, Iraq.

<sup>e</sup>Department of Biology, College of Science University of Misan, Maysan, Iraq.



CrossMark

### Abstract

The use of natural, eco-friendly coagulant-flocculants in wastewater treatment can help to reduce suspended particles in a way that includes less exhaustible materials with minimal adverse effects on the environment. Hence, this study is to investigate raw diatomaceous earth (diatomite) as a sustainable ecological coagulant to reduce colloids and suspended matter in wastewater and optimize the coagulation process parameters to improve efficiency, save energy consumption, and reduce costs in the urban sewage treatment plants. The Box-Behnken response surface design was applied to model the individual and combined interactions between four variable factors (initial pH, coagulant dose, coagulation speed, and coagulation time) and their effect on turbidity removal efficiency and final pH of water. Results showed that diatomite has excellent efficiency in reducing the turbidity of wastewater; Elimination reached a maximum of 85.74%. The optimal operating conditions for reducing energy consumption and cost of the operation while improving turbidity removal effectiveness and achieving a neutral final pH to avoid a post-adjustment are an initial pH of 7, a dose of diatomite of 0.5 g/L of effluent, and a coagulation speed of 100 rpm for 3 min. It results in 72.6% turbidity removal and a pH of 7.27. diatomaceous earth shows very usefully for reducing the turbidity of the sewage in the urban wastewater treatment plant.

**Keywords:** Wastewater; Process; Coagulation; Box-Behnken; Diatomite; Ecological; Environment.

### 1. Introduction

Water is one of the basic elements of sustainable development and its preservation is the protection of biodiversity on our planet. Growing urbanization and new modes of production and consumption in industrialized and developing countries create new challenges for managing the water cycle; wastewater sanitation is one of them [1]. It presents a dual challenge to public health and environmental protection; wastewater treatment plants are increasingly installed, and treatment technologies are being developed and improved [2]. The choice of technologies used depends essentially on the composition of the wastewater [3-8]. Nanotechnology, which deals with nanometre-sized objects (1-100 nm), has also been applied in a number of medical, biological, chemical, and wastewater treatment applications [9-14].

Aluminium and iron salts are the most frequently used coagulants [15,16]. However, significant aluminium and iron concentrations can persist in the treated water and cause some undesirable toxicity [17,18]. One way to cut down on traditional chemical coagulants and flocculants is to use new natural biomaterials that are biodegradable, non-toxic, and more environmentally friendly [19]. Thus, researchers are interested in designing, developing, and evaluating new natural or biomaterials with coagulant and flocculent effects [55-60].

Diatomaceous earth is a naturally occurring material formed by the accumulation of Bacillariophyceae, composed of fossilized diatom shells (SiO<sub>2</sub> about 70%) characterized by highly complex surface porosity (80–90% voids) with highly symmetrical patterns [20-22]. It is characterized by interesting mechanical and optical properties thanks to

\*Corresponding author e-mails: [benouiskhadidja@yahoo.fr](mailto:benouiskhadidja@yahoo.fr); (Khedidja Benouis) and [albukhaty.salim@uomisan.edu.iq](mailto:albukhaty.salim@uomisan.edu.iq); (Salim Albukhaty).

Receive Date: 23 April 2022, Revise Date: 06 May 2022, Accept Date: 11 May 2022

DOI: 10.21608/EJCHEM.2022.113005.5965

©2022 National Information and Documentation Center (NIDOC)

the pores' arrangement, size, and shape on their surfaces [9-12]. Diatom shells can be equally effectively used for biological and biomedical applications such as drug carriers [23,24] and sensing devices [20,25]. The Food and Drug Administration of the United States has authorized some diatomaceous earth as food-grade and added it to the list of food additives as an inert carrier or anti-caking agent in animal feed [21]. Diatomaceous earth is also employed in water treatment as a filter media [22,26] and as an adsorbent [27-36], but few studies have investigated the coagulant flocculent effect of diatomite alone [37] or mixed with other coagulants [37-42].

The aims of this study were:

- To assess the viability of using raw diatomite as a sustainable ecological bio-coagulant to reduce the turbidity of the sewage in the urban wastewater treatment plant.
- To optimize the coagulation process parameters using response surface methodology (RSM), including the dosage of diatomite in order to reduce costs and energy consumption while increasing the efficiency of the process.

The RSM is widely used to optimize water treatment processes. It integrates several factors and examines their interactions while reducing the number of experimental tests.

## 2. Material and Methods

### 2.1. Collection of sewage samples.

The samples were collected from the clarification basin of the municipal wastewater treatment plant (MWTP) in Sidi Bel Abbès in northwest Algeria. The city is geographically located at 35°11'38"N and 0°38'29"W and covers an area of 9150.63 km<sup>2</sup>. The population of Sidi Bel Abbes is 681190, with an estimated density of 72 inhabitants/km<sup>2</sup>; most of them are concentrated in the state's northwestern region [43]. The city's geography occupies a strategic middle position. It extends approximately 15% of the northwestern region and is centered between 05 states and crossed by most national roads. The MWTP receives urban wastewater and discharges from artisanal activities. The characteristics of the sewage are presented in Table 1.

**Table 1:** The characteristics of the sewage

parameter	pH	Electric conductivity (( $\mu$ s/cm)	TDS (mg/L)	Turbidity NTU
value	7.01	950	440	288

The raw effluent undergoes four stages of treatment before being returned to the receiving environment (Mekerra valley): desanding, coagulation-flocculation, biological filtration, and disinfection.

Using 1000 mL HDPE bottles, wastewater samples were taken at the inlet of the treatment plant's clarification tank. The water samples were stored and transported to the laboratory for analysis. The turbidity and pH of the wastewater were measured using an AQUALYTIC model AL250T-IR infrared turbidimeter and a HI-2211 benchtop pH and mV meter.

### 2.2. Experimental procedure of coagulation-flocculation.

The coagulation-flocculation tests were performed in a Jar Test apparatus (model AOUA / UTC) equipped with four stainless steel blades; the stirring speed varies from 0 to 200 rpm, while the stirring time is from 0 to 30 min.

A 600 ml beaker was filled with 400 ml of wastewater for each test. First, the wastewater's initial pH (pH<sub>i</sub>) was adjusted to the desired value using two solutions of 0.1N HCl and 0.1N NaOH. Then, a dose of diatomite varying between 0.5 and 3 g/L was added. Coagulation speed and time varied depending on the design (50, 150, and 200 rpm for 3, 5, and 7 min). Then, the speed of stirring was reduced to 20 rpm for 20 min to promote the formation of flocs (flocculation). After flocculation, the samples were left to stand for 60 minutes. Then, 300 ml of the supernatant was removed using a dipstick for analysis. equation (1) was used to calculate the rate of turbidity removal, which was expressed as a percentage.

$$\text{Turbidity removal efficiency (\%)} = \frac{1 - (\text{final turbidity} / \text{initial turbidity})}{1} * 100 \quad (1)$$

### 2.3. Experimental design.

A statistical optimization was carried out to minimize the energy consumed during the coagulation operation while improving the rate of elimination of turbidity and making the final pH of the water tend towards neutrality to avoid a possible post pH adjustment. Response surface methodology (RMS) was employed to study mutual interaction effects among the selected operating parameters using the Box-Behnken design (BBD) Design-Expert® software. The impact of four variable factors: initial pH (X<sub>1</sub>), the dose of diatomite (X<sub>2</sub>), the coagulation speed (X<sub>3</sub>), and the coagulation time (X<sub>4</sub>) on the

efficiency of turbidity removal ( $Y_1$ ) and the final pH ( $Y_2$ ) was studied.

Ranges of the variables have been set according to experiments previously carried out. The values are presented in Table 2.

**Table 2:** Experimental range and levels of variables

Coded factors	Factors	Unit	Coded levels		
			-1	0	+1
$X_1$	Initial pH	-	4	7	10
$X_2$	Dose of diatomite	g/L	0.5	1.75	3
$X_3$	Coagulation speed	rpm	100	150	200
$X_4$	Coagulation time	mn	3	5	7

The number of tests ( $n$ ) required to generate Box Behnken Design is specified as follows:

$$n = 2f(f-1) + Cp \quad (2)$$

$f$  and  $Cp$  denote the number of factors and the number of central points, respectively.

Experiments were carried out randomly to reduce systematic error; furthermore, three center replicates were inserted to evaluate the pure experimental error and improve the model's design. A total of 27 experiments were performed, and the obtained and predicted responses achieved are shown in Table 3. The relationships between responses and independent variables and predict the optimal coagulation-flocculation process conditions were established using an empirical second-order polynomial model (equation 3).

$$Y = a_0 + \sum_{i=1}^k a_i X_i + \sum_{i=1}^k a_{ii} X_i^2 + \sum_{i=1}^{k-1} \sum_{j=2}^k a_{ij} X_i X_j + e \quad (3)$$

Design-Expert software was used for the design of the experiment, estimation of the coefficients, analysis of data, and plotting of graphs.

### 3. Results and Discussion

#### 3.1. Characterization of the raw diatomite.

The diatomite used in this study was collected from the TAHLAIT ENOF deposit, located 5 km from the Sig area in Algeria. It is a light, powdery rock that is brilliantly white. The raw diatomite sample was crushed, air-dried, finely ground, and finally sieved. The sample's chemical composition was identified using x-ray fluorescence spectrometer (model Rigaku ZSX Primus II).  $SiO_2$  has been identified as the most predominant constituent, and the main minor

components are calcium oxide and metal oxides ( $CaO$ ,  $Al_2O_3$ , and  $Fe_2O_3$ ) (Table 4).

FT-IR analyses in the 400–4000  $cm^{-1}$  range were performed using an Alpha Bruker FT-IR spectrometer to investigate the surface characteristics of the raw diatomite. The infrared spectra illustrated in Figure 1 show the prominent absorption bands. The bands at 998, 872, 792, 689, 521, and 460  $cm^{-1}$  were particularly noticeable. The band at 998  $cm^{-1}$  corresponds to the siloxane group's ( $-Si-O-Si-$ ) elongation, whereas the band at 872  $cm^{-1}$  corresponds to the silanol group's  $Si-O$  elongation. The bands at 792 and 689  $cm^{-1}$  are assigned to the vibrations of the  $SiO-H$  bonding, and Absorption peaks at 521 and 460  $cm^{-1}$  are attributed to  $Si-O-Si$  bending vibrations [44,45]. X-ray analysis identified the crystalline phases using a Siemens D5000 diffractometer utilizing  $g\ CuK\alpha_1$  radiation in the Bragg Brentano configuration. The XR- diffractogram of diatomite is shown in Figure 2. The prominent peaks correspond to quartz, calcite, cristobalite, and a mixture of kaolinite, smectite, and hematite [46-48].

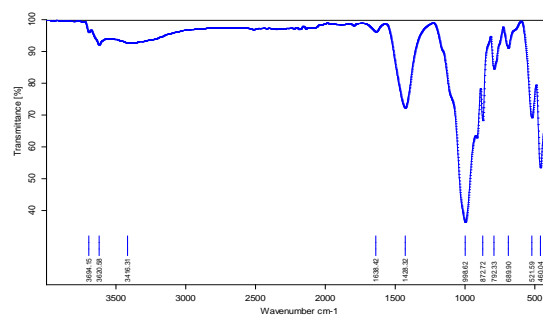


**Figure 1.** FT-IR spectra of the raw powder diatomite

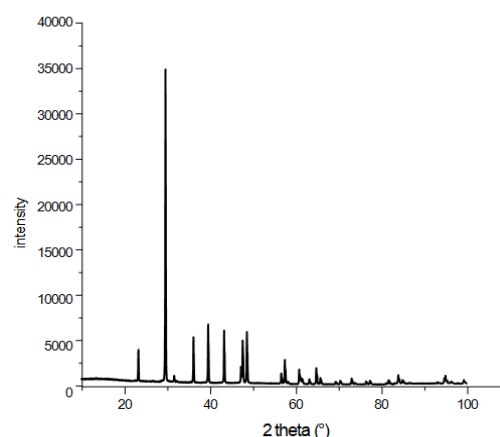


**Figure 2.** XR- Diffractogram of raw powder diatomite

**Table 3:** Experimental conditions of Variables and response

Run	Factors				Responses			
	X <sub>1</sub>	X <sub>2</sub>	X <sub>3</sub>	X <sub>4</sub>	Y <sub>1</sub>		Y <sub>2</sub>	
	Initial pH	Dose of diatomite (g/L)	Coagulation speed (rpm)	Coagulation time (min)	Turbidity removal (%)		Final pH	
					Actual	predicted	Actual	predicted
1	7	1.75	150	5	75.55	74.13	7.19	7.20
2	7	1.75	200	3	72.96	73.43	7.21	7.31
3	7	1.75	100	3	74.07	73.41	7.27	7.32
4	4	3.00	150	5	66.66	66.26	6.62	6.74
5	10	3.00	150	5	83.33	83.78	9.60	9.44
6	7	1.75	100	7	73.7	73.78	7.32	7.31
7	7	0,50	150	7	74.44	72.75	7.17	7.17
8	10	0.50	150	5	84.26	85.20	9.63	9.60
9	10	1.75	150	7	85.74	85.79	9.65	9.60
10	4	1.75	150	3	62.96	64.38	6.7	6.68
11	10	1.75	150	3	82.4	83.01	9.65	9.61
12	7	1.75	200	7	72.22	73.43	7.28	7.32
13	10	1.75	100	5	84.72	84.08	9.52	9.67
14	7	1.75	150	5	72.77	74.13	7.21	7.20
15	4	1.75	200	5	64.07	62.69	6.93	6.76
16	7	3.00	150	7	75.55	75.03	7.23	7.28
17	10	1.75	200	5	85.74	84.33	9.43	9.56
18	7	3.0	100	5	73.51	74.09	7.25	7.27
19	4	1.75	100	5	63.88	63.27	6.8	6.65
20	7	1.75	150	5	74.07	74.13	7.21	7.20
21	4	1.75	150	7	61.11	61.97	6.74	6.71
22	7	0.50	200	5	70.74	71.64	7.30	7.21
23	7	3.0	150	3	75.18	74.85	7.24	7.22
24	4	0.50	150	5	60.18	60.28	6.21	6.47
25	7	0.50	150	3	74.07	72.57	7.29	7.22
26	7	0.50	100	5	72.03	73.28	7.25	7.19
27	7	3	200	5	75.18	75.40	7.25	7.24

**Table 4:** Chemical composition of the raw diatomite powder

Oxide	SiO <sub>2</sub>	CaO	Al <sub>2</sub> O <sub>3</sub>	Fe <sub>2</sub> O <sub>3</sub>	K <sub>2</sub> O	MgO	Na <sub>2</sub> O	TiO <sub>2</sub>	Fire losses
Wt %	69.07	15.42	6.14	2.73	1.70	1.18	0.14	0.085	3.5

### 3.2. Statistical analysis

Analysis of variance (ANOVA) was utilized to examine the relationships among factors, their possible interactions, and their impacts on responses and validate and determine the significance of the developed models. ANOVA analysis indicated that the linear model was highly significant for the response Y<sub>1</sub>, while the quadratic was selected to be more appropriate for the response Y<sub>2</sub>. Summary statistics for the models are summarized in Table 5. The first statistical analysis is by the F and p values. The model F-value of 159.58 and 109.01 and the model p-values of under 0.0001 for the linear and quadratic models are less than 0.05, implying that the models were significant (Tables 6 and 7). The factors significantly impacting turbidity removal

and final pH are also given in tables 6 and 7. For the turbidity removal, initial pH (X<sub>1</sub>) and the mass of diatomite (X<sub>2</sub>) were significant terms (p < 0.05). For the final pH of the effluent, its initial pH (X<sub>1</sub>) and quadratic initial pH (X<sub>1</sub><sup>2</sup>) were significant terms.

The linear and quadratic equations used to explain the removal of turbidity (Y<sub>1</sub>) and the final pH of water (Y<sub>2</sub>) are represented in equations 4 and 5, respectively. Equations were adjusted by removing terms that were judged to be statistically insignificant. The mathematical equations obtained were used to analyze the goodness of fit.

$$Y_1 = 51.33626 + 3.31635 X_1 + 0.220452 X_2 \quad (4)$$

$$Y_2 = 8.60766 - 0.807461 X_1 + 0.099352 X_1^2 \quad (5)$$

The predicted and experimental values of  $Y_1$  and  $Y_2$  presented in Figure 3 are in close agreement. In addition, the data points are well dispensed along the  $45^\circ$  axis, indicating that the models developed for the turbidity removal and the final pH were well-suited for forming a relationship between independent and dependent variables.

The coefficient of determination Regression ( $R^2$ ) responses  $Y_1$  and  $Y_2$  was found to be 0.9667 and 0.9922, respectively (Table 8), which means that the total variation explained by the developed models was 96.67 and 99.22 %; this indicates that the dependent and independent variables were in a reliable relationship. On the other hand, there might be 3.33 and 0.78 % of the total variation, which could not be explicated by the models developed. Compared to prior research adopting Response Surface Methodology to improve the coagulation step in wastewater treatment, the high correlations between experimental and predicted data indicated that our models could be judged highly significant [49-54,61-66].

**Table 5:** Model Summary Statistics

	source	p-value	$R^2$	$R^2_{adj}$	$R^2_{pred}$	
Turbidity removal	<b>Linear</b>	<b>&lt; 0.0001</b>	<b>0.9667</b>	<b>0.9606</b>	<b>0.9490</b>	<b>Suggested</b>
	2FI	0.0660	0.9828	0.9721	0.9494	
	Quadratic	0.9730	0.9835	0.9642	0.9146	
	Cubic	0.9786	0.9880	0.9219	-0.3422	Aliased
Final pH	Linear	< 0.0001	0.8223	0.7900	0.7287	
	2FI	0.9998	0.8244	0.7146	0.4525	
	<b>Quadratic</b>	<b>&lt; 0.0001</b>	<b>0.9922</b>	<b>0.9831</b>	<b>0.9551</b>	<b>Suggested</b>
	Cubic	0.1086	0.9991	0.9940	0.8691	Aliased

The predicted  $R^2$  values for responses  $Y_1$  and  $Y_2$  were 0.9490 and 0.9551, respectively (Table 7), which were close to the  $R^2$  values (0.9667 and 0.9922, respectively). They are also in good agreement with the RMS adjusted  $R^2$  values of 0.9606 and 0.9831 for turbidity removal ( $Y_1$ ) and final pH ( $Y_2$ ), respectively; the difference is less than 0.2.

Adequate Precision (A.P) measures the experimental signal-to-noise ratio. It is preferable to have a ratio that exceeds four. The AP score was 37.326 and 30.288 for  $Y_1$  and  $Y_2$ , respectively. That reflected an adequate signal and indicated that the model would perform admirably (table 8). The standard deviation (S.D) and coefficient of variation (C.V) indicate the degree of precision the experiments are compared. The lower values of S.D (1.46 and 0.1419 for  $Y_1$  and  $Y_2$ , respectively) and C.V (1.98% and 1.86% for  $Y_1$  and  $Y_2$ , respectively) imply good precision and reliability of the experiments and indicate that the models are reasonably reproducible (Table 8).

**Tables 6:** ANOVA for linear model (Response  $Y_1$ )

source	df*	SS*	MS*	F-value	p-value	
<b>Model</b>	4	1366.70	341.67	159.58	< 0.0001	sign**
<b><math>X_1</math>-initial pH</b>	1	1350.87	1350.87	630.93	< 0.0001	sign**
<b><math>X_2</math>- dose of diatomite</b>	1	15.64	15.64	7.31	0.0130	sign**
<b><math>X_3</math>- coagulation speed</b>	1	0.0867	0.0867	0.0405	0.8424	no sign**
<b><math>X_4</math>-coagulation time</b>	1	0.1045	0.1045	0.0488	0.8272	no sign**
<b>Residual</b>	22	47.10	2.14			
<b>Cor Total</b>	26	1413.80				

**Table 7:** ANOVA for quadratic model (Response  $Y_2$ )

source	df*	SS*	MS*	F-value	p-value	
Model	14	30.74	2.20	109.01	< 0.0001	sign**
$X_1$ -initial pH	1	25.46	25.46	1264.30	< 0.0001	sign**
$X_2$ - dose of diatomite	1	0.0096	0.0096	0.4783	0.5023	no sign**
$X_3$ - coagulation speed	1	8.333E-06	8.333E-06	0.0004	0.9841	no sign**
$X_4$ -coagulation time	1	0.0001	0.0001	0.0037	0.9523	no sign**
$X_1 X_2$	1	0.0484	0.0484	2.40	0.1470	no sign**
$X_1 X_3$	1	0.0121	0.0121	0.6008	0.4533	no sign**
$X_1 X_4$	1	0.0004	0.0004	0.0199	0.8903	no sign**
$X_2 X_3$	1	0.0006	0.0006	0.0310	0.8631	no sign**
$X_2 X_4$	1	0.0030	0.0030	0.1502	0.7051	no sign**
$X_3 X_4$	1	0.0001	0.0001	0.0050	0.9450	no sign**
$X_1^2$	1	4.26	4.26	211.73	< 0.0001	sign**
$X_2^2$	1	0.0068	0.0068	0.3400	0.5706	no sign**
$X_3^2$	1	0.0195	0.0195	0.9666	0.3449	no sign**
$X_4^2$	1	0.0149	0.0149	0.7415	0.4060	no sign**
Residual	12	0.2417	0.0201			
Cor Total	26	30.98				

\*: *df*: degree of freedom, *SS*: Sum of Squares, *MS*: Mean Square \*\*: sign: significant, no sign: non-significant

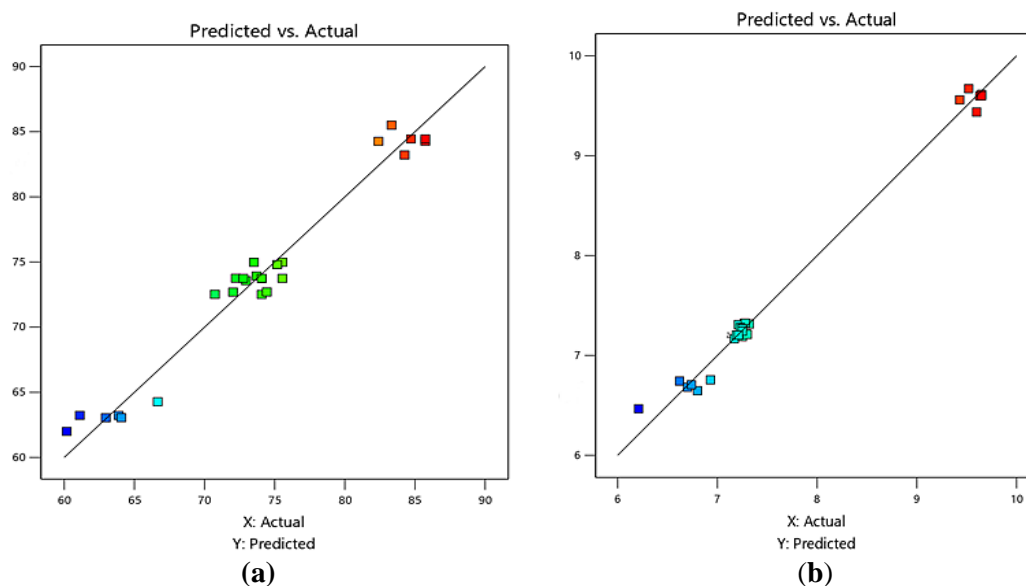


**Figure 3.** Predicted vs. actual plot for turbidity removal (a); final pH (b)

**Table 8:** Statistical parameters for responses  $Y_1$  and  $Y_2$

	$Y_1$ Turbidity removal (%)	$Y_2$ Final pH
$R^2$	0.9667	0.9922
Adjusted $R^2$	0.9606	0.9831
Predicted $R^2$	0.9490	0.9551
Adequate Precision A.P	37.3261	30.2879
Standard Deviation S.D	1.46	0.1419
Coefficient of Variation C.V. %	1.98	1.86

### 3.3. Process optimization.

A numerical optimization analysis was performed using BBD. The objective was to minimize the energy consumed and the cost of coagulation treatment while ensuring good turbidity removal efficiency. The objectives and limitations of the optimization are reported in Table 9.

The initial and final pH levels were targeted to 7 to avoid a pH adjustment step before or after coagulation treatment. Speed and time of coagulation and the dose of diatomite were minimized throughout the range of variation of each factor to reduce energy consumption. The selected optimal conditions were: an initial pH of 7, a dose of diatomite of 0.5g/L, coagulation speed of 100 rpm, and coagulation time of 3 min (Figure 4).

At these optimal conditions, the predicted removal of turbidity obtained is 72.60%, and the final pH is 7.27, a pH close to neutral, which does not

require post adjustment. The desirability of these optimal conditions is 0.992 (Figure 5). The 3D graph of this desirability is shown in Figure 6.

In order to explain the independent variables' effects and interactions, 2D contour and 3D response surface plots were made as a function of two variables with the remaining variables held constant at optimal conditions. The behavior of turbidity removal and final pH is illustrated in the graphs shown in Figures 7 and 8. Parallel and well-spaced curvatures are observed, which affirm a positive relationship between the two variables, initial pH ( $X_1$ ) and the dose of the diatomite ( $X_2$ ), of linear profile for the turbidity removal efficiency ( $Y_1$ ) and quadratic for the final pH ( $Y_2$ ) (Figures 7).

The 3D response surface plots of  $Y_1$  and  $Y_2$  at the optimum condition ( $X_3$ : 100 rpm and  $X_4$ : 3 min) are shown in Figure 8. The initial pH was the

most influential and effective parameter on diatomite performance. The maximum reduction in turbidity was observed at high pH and the low mass of diatomite. The turbidity removal rate has increased to reach its maximum (85.74%) at pH 10 and a diatomite dose of 3 g/L (figure 8a). The optimal point was not observed at the highest reduction rate due to the objectives set for the optimization. The optimum

point was reached at 72.60% turbidity removal for a  $pH_i$  of 7 and a diatomite dose of 0.5g/L.

The final pH of wastewater strongly depended on its initial pH; an increase in  $pH_i$  induced an increase in  $pH_f$ . Independent of diatomite mass, minimum and maximum  $pH_f$  were reached at the lowest and highest  $pH_i$ . The  $pH_f$  range was minimal, with an increase in diatomite mass as shown in Figure 8b.

**Table 9:** Objectives and ranges of optimization

Symbol	Factor	Unit	Aim	Minimum level	Maximum level
X <sub>1</sub>	Initial pH	-	target to 7	4	10
X <sub>2</sub>	dose of diatomite	g/L	minimize	0.5	3
X <sub>3</sub>	coagulation Speed	rpm	minimize	100	200
X <sub>4</sub>	coagulation Time	min	minimize	3	7
Y <sub>1</sub>	turbidity removal	%	in range	70	100
Y <sub>2</sub>	final pH	-	target to 7	0	14

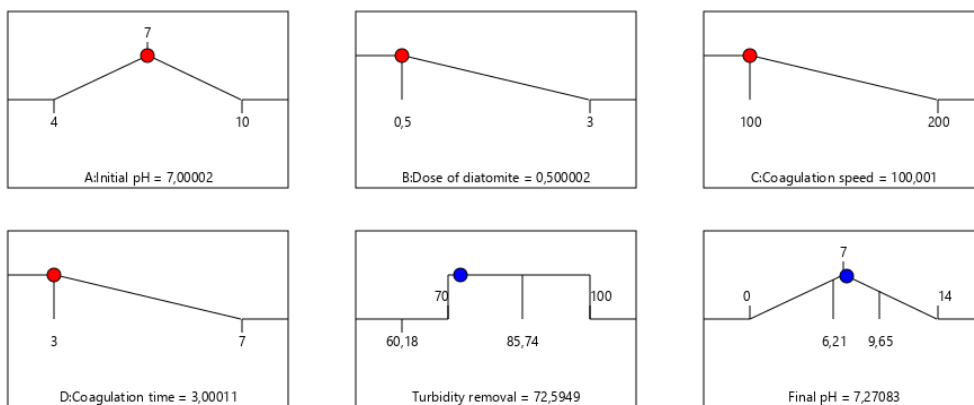


**Figure 4.** predicted solution obtained by numerical optimization

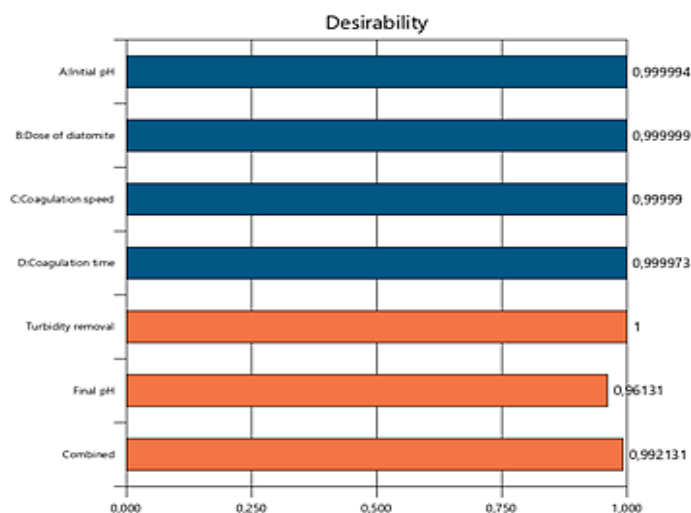


**Figure 5.** Bar graph of desirability using Design-Expert v13

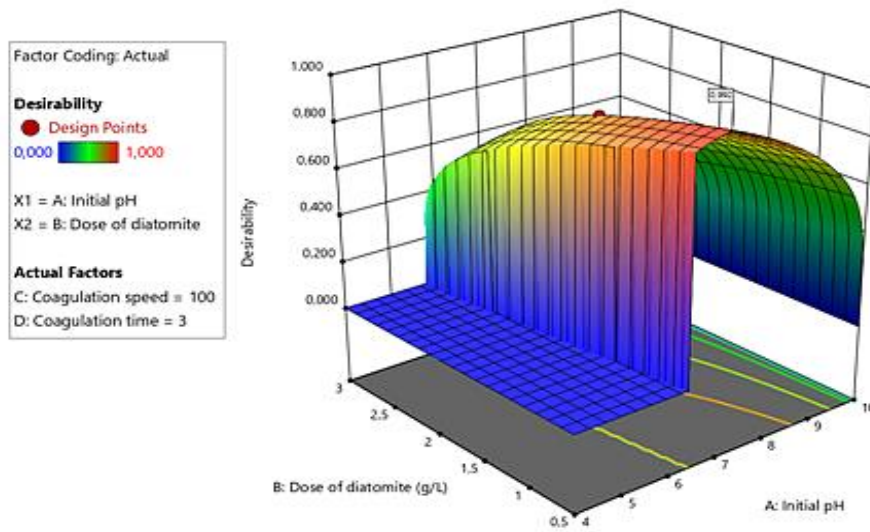


Figure 6. Desirability surface for optimal conditions using Design-Expert v13 software. The three-dimension response surface plots (3D).

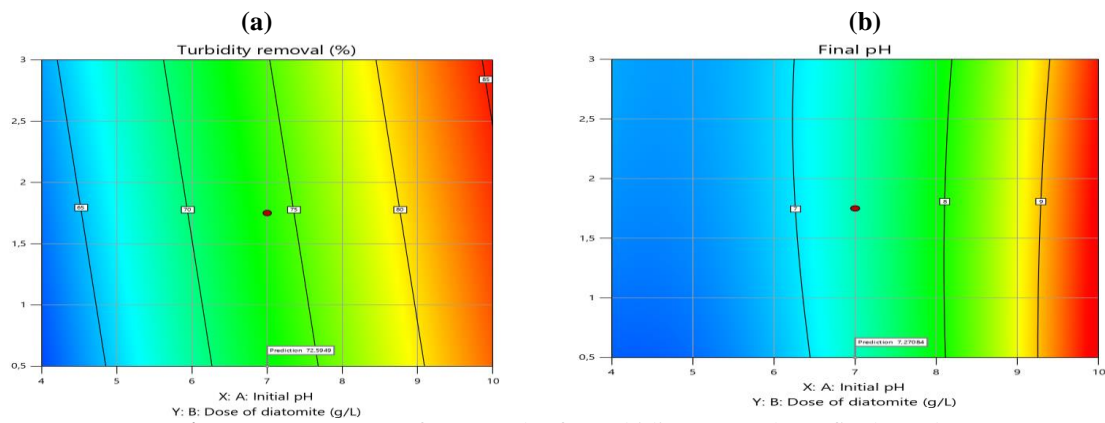


Figure 7. response surface 2D-plot for turbidity removal (a); final pH (b)

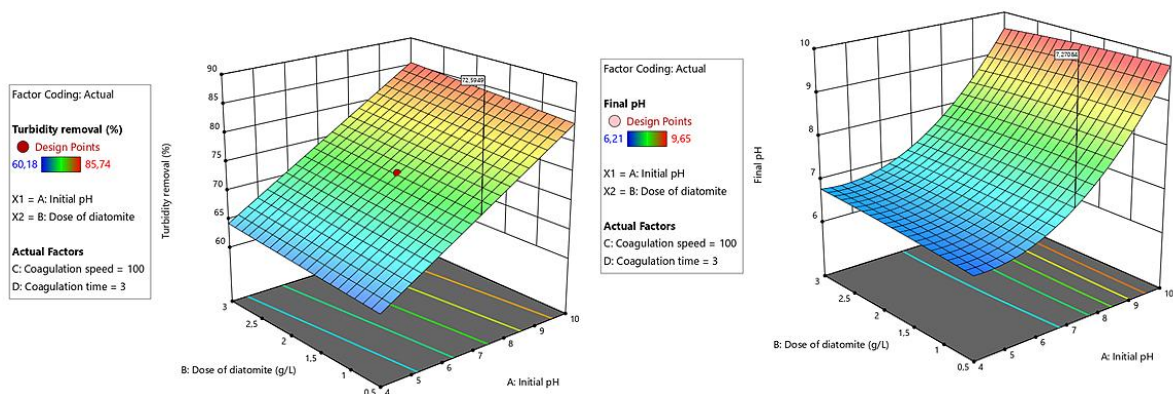


Figure 8. response surface 3D-plot for (a) turbidity removal; (b) final pH

#### 4. Conclusions

This study exploited the experimental design methodology to evaluate the performance of crude diatomaceous earth as a natural ecological coagulating agent and optimize process parameters to reduce energy consumption in the municipal water treatment plant. As a result, it was possible to achieve optimum efficiency of 85.74% turbidity removal using diatomite coagulant. Under optimum conditions, 72.60 was reached, and the final pH of the water tended to be 7.27. Furthermore, no initial pH adjustment was necessary to achieve these results. In addition, the dose of diatomite used and the speed and time of agitation during the coagulation phase were the lowest, which made it possible to save as much energy and cost of treatment as possible while still getting rid of more than 70% of suspended solids expressed in terms of turbidity. The application of this inexpensive natural agent can overcome the challenges related to suspended solids and colloidal particles responsible for the turbidity of wastewater. The recorded correlation between experimental and predicted responses was perfect. In addition, The BBD models developed presented high correlation coefficient ( $R^2$ ) values, 96% for turbidity reduction efficiency and 99% for final water pH, respectively, indicating the excellent adequacy of both quadratic and linear models and correctly describing the interaction between all the factors involved.

These results showed that the response surface methodology could be successfully used to simulate and optimize the coagulation process in the step of the clarification of wastewater. Furthermore, it is economical and provides the most accuracy and information in the shortest time with the fewest experiments. Using natural materials and limiting energy consumption in the wastewater treatment plant reduces the pollution generated, allows the installation's proper operation, and increases its lifespan while improving the process's performance.

#### 5. Conflicts of interest

“There are no conflicts to declare”.

#### 6. Acknowledgments

The authors wish to thank the responsible staff of the municipal wastewater treatment plant

(WWTP) of Sidi Bel Abbès in Algeria for their collaboration.

#### 7. References

- [1] Larsen, T.A.; Hoffmann, S.; Lüthi, C.; Truffer, B.; Maurer, M. Emerging solutions to the water challenges of an urbanizing world. *Science* **2016**, *352*, 928–933.
- [2] Wang, X.-H.; Wang, X.; Huppel, G.; Heijungs, R.; Ren, N.-Q. Environmental implications of increasingly stringent sewage discharge standards in municipal wastewater treatment plants: Case study of a cool area of China. *J. Clean. Prod.* **2015**, *94*, 278–283.
- [3] Capodaglio, A.G. Integrated, Decentralized Wastewater Management for Resource Recovery in Rural and Peri-Urban Areas. *Resources* **2017**, *6*, 22.
- [4] Abdel-Shafy HI. Chemical treatment for removal of heavy metals from industrial wastewater. *Egypt J Chem.* 2015 Jan 1;58(1):1-2.
- [5] Nasr F, Abdelfattah I, Shana A. Cost-effective Physicochemical Treatment of Carpet Industrial Wastewater for Reuse. *Egyptian Journal of Chemistry.* 2019 Apr 1;62(4):609-20.
- [6] El-Awady MH, El-Ghetany HH, Aboelghait KM, Dahaba AA. Zero liquid discharge and recycling of paper mill industrial wastewater via chemical treatment and solar energy in Egypt. *Egyptian Journal of Chemistry.* 2019 Dec 1;62(Special Issue (Part 1) Innovation in Chemistry):37-45.
- [7] Nikpor A, Ghorbania HR. Investigating the effect of coagulants and nano-coagulants to reduce biological oxygen demands in industrial wastewater. *Egyptian Journal of Chemistry.* 2021 Sep 1;64(9):4809-13.
- [8] Ghorbani HR, Nikpor A. The study of TSS reduction in industrial wastewater by nano-coagulants. *Egyptian Journal of Chemistry.* 2022 Apr 1;65(4):315-320.
- [9] Alyamani, A.A.; Albukhaty, S.; Aloufi, S.; AlMalki, F.A.; Al-Karagoly, H.; Sulaiman, G.M. Green Fabrication of Zinc Oxide Nanoparticles Using *Phlomis* Leaf Extract: Characterization and In Vitro Evaluation of Cytotoxicity and Antibacterial Properties. *Molecules* **2021**, *26*, 6140.
- [10] Khashan, K.S.; Sulaiman, G.M.; Abdulameer, F.A.; Albukhaty, S.; Ibrahim, M.A.; Al-Muhimeed, T.; AlObaid, A.A. Antibacterial Activity of TiO<sub>2</sub> Nanoparticles Prepared by One-

- Step Laser Ablation in Liquid. *Appl. Sci.* **2021**, *11*, 4623
- [11] Safat, S.; Buazar, F.; Albukhaty, S.; Matroodi, S. Enhanced sunlight photocatalytic activity and biosafety of marine-driven synthesized cerium oxide nanoparticles. *Sci. Rep.* **2021**, *11*, 14734.
- [12] Honda, R.J.; Keene, V.; Daniels, L.; Walker, S.L. Removal of TiO<sub>2</sub> nanoparticles during primary water treatment: Role of coagulant type, dose, and nanoparticle concentration. *Environ. Eng. Sci.* **2014**, *31*, 127–134.
- [13] Aldujaili NH, Banoon SR. Antibacterial characterization of titanium nanoparticles nano synthesized by *Streptococcus thermophilus*. *Periodico Tch Quimica (Online)*. **2020**;17(34):311-20.
- [14] Banoon SR, Ghasemian A. The characters of graphene oxide nanoparticles and doxorubicin against HCT-116 colorectal cancer cells in vitro. *Journal of Gastrointestinal Cancer*. **2021** Mar 19:1-5.
- [15] Brandt, M. J.; Johnson, K. M.; Elphinston, A. J.; Ratnayaka, D.D. Storage, Clarification and Chemical Treatment. *Twort's Water Supply (Seventh Edition) 2017*, 323–366.
- [16] Dassanayake, K.B.; Jayasinghe, G.Y.; Surapaneni, A.; Hetherington, C. A review on alum sludge reuse with special reference to agricultural applications and future challenges. *Waste Management* **2015**, *38*(1), 321–335.
- [17] Shi, B.; Li, G.; Wang, D.; Feng, C.; Tang, H. Removal of direct dyes by coagulation: The performance of preformed polymeric aluminum species. *J. Hazard. Mater.* **2007**, *143*, 567–574.
- [18] Kweiner Tetteh, E.; Rathilal, S. Kinetics and Nanoparticle Catalytic Enhancement of Biogas Production from Wastewater Using a Magnetized Biochemical Methane Potential (MBMP) System. *Catalysts* **2020**, *10*, 1200.
- [19] Owodunni, A.A.; Suzylawati, I. Revolutionary technique for sustainable plant-based green coagulants in industrial wastewater treatment—A review. *Water Process Eng.* **2021**, *42*, 102096.
- [20] Villani, M.; Onesto, V.; Coluccio, M.; Valpapuram, I.; Majewska, R.; Alabastri, A.; Battista, E.; Schirato, A.; Calestani, D.; Coppedé, N.; Zappettinia, A.; Amato, F.; Fabrizio, E.D.; Gntile, F.; Transforming diatomaceous earth into sensing devices by surface modification with gold nanoparticles. *Micro Nano Eng* **2019**, *2*, 29–34.
- [21] Bradbury, J. Nature's nanotechnologists: unveiling the secrets of diatoms. *PLoS Biol* **2004**, *2*, 1512-1515.
- [22] Mishra, M.; Arukha, A.P.; Bashir, T.; Yadav, D.; Prasad, G.B.K.S., All new faces of diatoms: Potential source of nanomaterials and beyond. *Front. Microbiol.* **2017**, *8*, 1–8.
- [23] Sardo A, Orefice I, Balzano S, Barra L, Romano G. Mini-review: potential of diatom-derived silica for biomedical applications. *Applied Sciences*. **2021** Jan;11(10):4533.
- [24] Delasoie J, Zobi F. Natural diatom biosilica as microshuttles in drug delivery systems. *Pharmaceutics*. **2019** Oct;11(10):537.
- [25] Sharma N, Simon DP, Diaz-Garza AM, Fantino E, Messaabi A, Meddeb-Mouelhi F, Germain H, Desgagné-Penix I. Diatoms biotechnology: various industrial applications for a greener tomorrow. *Frontiers in Marine Science*. **2021** Feb 23;8:106.
- [26] Ferrara, M.A.; Dardano, P.; De Stefano, L.; Rea, I.; Coppola, G.; Rendina, I.; Congestri, R.; Antonucci, A.; De Stefano, M.; De Tommasi E. Optical properties of diatom nanostructured biosilica in *Arachnoidiscus* sp: micro-optics from mother nature. *PLoS One* **2014**, *9*.
- [27] Romann, J.; Valmalette, J.C.; Chauton, M.S.; Tranell, G.; Einarsrud, M.A.; Vadstein, O. Wavelength and orientation dependent capture of light by diatom frustule nanostructures. *Sci Rep* **2015**, *5*, pp. 1-6.
- [28] Romann, J.; Valmalette, J.C.; Røyset, A.; Einarsrud, M.A. Optical properties of single diatom frustules revealed by confocal microspectroscopy. *Opt. Lett* **2015**, *40*, 740–743,
- [29] Yamanaka, S.; Yano, R.; Usami, H.; Hayashida, N.; Ohguchi, M.; Takeda, H.; Yoshino, K. Optical properties of diatom silica frustule with special reference to blue light. *J. Appl. Phys* **2008**, *103*, 074701.
- [30] Saxena, A.; Dutta, A.; Kapoor, N.; Kumar, A.; Tiwari, A. Envisaging marine diatom *Thalassiosira weissflogii* as a "SMART" drug delivery system for insoluble drugs. *J Drug Deliv Sci Technol* **2022**, *68*, 102983.
- [31] Sakshi P.; Abhishek S.; Neha K.; Charu A.; Archana T. Diatom mediated smart drug delivery system, *J Drug Deliv Sci Technol* **2021**, *63*, 102433.
- [32] Uthappa, U.T.; Brahmkhatri, V.; Sriram, G.; Jung, H.Y.; Yu, J.; Kurkuri, N.; Aminabhavi, T.M.; Altalhi, T.; Neelgund, G.M.; Kurkuri,

- M.D. Nature engineered diatom biosilica as drug delivery systems. *JCR* **2018**, 281, 70-83.
- [33] Villani, M.; Onesto, V.; Coluccio, M.L.; Valpapuram, I.; Majewska, R.; Alabastri, A.; Battista, E.; Schirato, A.; Calestani, D.; Coppedé, N.; Zappettini, A.; Amato, F. Di Fabrizio, E.; Gentile, F. Transforming diatomaceous earth into sensing devices by surface modification with gold nanoparticles, *Micro Nano Eng* **2019**, 2, 29-34.
- [34] Gonzaga, F.L.L.; Gouveia J. F.S.; Karine Medeiros Holanda, A.I.M. Moreira de Carvalho, I.M.; Longhinotti, E.; Paulo, T.F.; Abreu, D.S.; Bernhardt, P.V.; Gilles-Gonzalez, M.A.; Cirino Nogueira Diógenes, M. E.H.S. Sousa, E.H.S. Bioinorganic systems responsive to the diatomic gases O<sub>2</sub>, NO, and CO: From biological sensors to therapy, *Coord Chem Rev* **2021**, 445, 214096.
- [35] Esfandyari, J.; Shojaedin-Givi, B.; Hashemzadeh, H.; Mozafari-Nia, M.; Vaezi, Z.; Naderi-Manesh, N. Capture and detection of rare cancer cells in blood by intrinsic fluorescence of a novel functionalized diatom, *Photodiagnosis Photodyn Ther* **2020**, 30, 2, 101753.
- [36] US food and drug administration (FDA), Code of Federal Regulations, Title 21-FOOD And Drugs, Chapter I-Food And Drug Administration, Department Of Health And Human Services, Volume 6.
- [37] Guo, d.; Wang, H.; Fu, P.; Huang, Y.; Liu, Y.; Lv, W.; Wang, F. Diatomite precoat filtration for wastewater treatment: Filtration performance and pollution mechanisms, *Chem Eng Res Des* **2018**, 137, 403-411.
- [38] Xu, L.; Gao, X.; Li, Z.; Gao, C. Removal of fluoride by nature diatomite from high-fluorine water: An appropriate pretreatment for nanofiltration process, *Desalination* **2015**, 369, 97-104.
- [39] Marthi, R.; Smith, Y.R. Selective recovery of lithium from the Great Salt Lake using lithium manganese oxide-diatomaceous earth composite. *Hydrometallurgy* **2019**, 186, 115-125.
- [40] Plata-Gryl, M.; Momotko, M.; Makowiec, S.; Boczkaj, G. Characterization of diatomaceous earth coated with nitrated asphaltenes as superior adsorbent for removal of VOCs from gas phase in fixed bed column, *Chem. Eng. J* **2022**, 427, 130653.
- [41] Wang, B.; Xiong, M.; Shi, B.; Li, Z.; Zhang, H. Treatment of shale gas flowback water by adsorption on carbon-nanotube-nested diatomite adsorbent. *J. Water Process* **2021**, 42, 102074.
- [42] Baba, F.; Benaliouche, F.; Meknaci, R.; Boucheffa, Y. Water adsorption and antibacterial activity studies for characterization of Ca-LTA zeolite/diatomite adsorbents, *Colloid and Interface Science Communications* **2020**, 35, 100233.
- [43] Mahfoud, Z., Khaldi, A., & Korichi, K. Wastewater reuse and mapping of irrigable soils: Case of Sidi Bel Abbes City, Algeria. *Journal of Water and Land Development*, 2020, (46), 153-161.
- [44] Hayakawa, S.; Hench, L.L. AMI study on infrared spectra of silica clusters modified by fluorine. *J. Non Crystalline Solids* 2000, 262, 264-270.
- [45] Khraisheh, M. A. M.; Al-Ghouti, M. A.; Allen, S. J.; Ahmad, M. N. Effect of OH and silanol groups in the removal of dyes from aqueous solution using diatomite. *Water Research* 2005, 39, 922-932.
- [46] Hadjadj-Aoul, O.; Belabbes, R.; Belkadi, M.; & Guermouche, M. H. Characterization and performances of an Algerian diatomite-based gas chromatography support. *Appl. Surf. Sci* 2018, 240, 131-139.
- [47] Benkacem, T.; Hamdi, B.; Chamayou, A.; Balard, H.; Calvet, R. Physicochemical characterization of a diatomaceous upon an acid treatment: a focus on surface properties by inverse gas chromatography. *Powder Technol* 2016, 294, 498-507.
- [48] Aouadja, F., Bouzerara, F., Guvenc, C. M., & Demir, M. M. Fabrication and properties of novel porous ceramic membrane supports from the (Sig) diatomite and alumina mixtures. *BOL SOC ESP CERAM V* 2021, In press.
- [49] G. Louhichi, L. Boussemli, A. Ghrabi, Process optimization via response surface methodology in the physico-chemical treatment of vegetable oil refinery wastewater, *Environ Sci Pollut Res*, 2019, pp. 18993-19011.
- [50] Ö.B. Gökçek, S. Özdemir, Optimization of the Coagulation-Flocculation Process for Slaughterhouse Wastewater Using Response Surface Methodology, *Clean – Soil, Air, Water*, 2020.
- [51] N.M. Daud, S. R. Sheikh Abdullah, H. Abu Hasan. Response surface methodological analysis for the optimization of acid-catalyzed

- transesterification biodiesel wastewater pre-treatment using coagulation–flocculation process, *Process Safety and Environmental Protection*, Volume 113, 2018, Pages 184-192.
- [52] N. M. Huzir, M. M.A. Aziz, S.B. Ismail, N. A.N. Mahmood, N.A. Umor, S. A. F.S. Muhammad, Optimization of coagulation-flocculation process for the palm oil mill effluent treatment by using rice husk ash, *Industrial Crops and Products*, Volume 139, 2019, 111482.
- [53] H.S. Kusuma, A.N. Amenaghawon, H. Darmokoesoemo, Y.A.B. Neolaka, B. Ayu Widyaningrum, CL. Anyalewechi, P. I.Orukpe, Evaluation of extract of Ipomoea batatas leaves as a green coagulant–flocculant for turbid water treatment: Parametric modelling and optimization using response surface methodology and artificial neural networks, *Environmental Technology & Innovation*, Volume 24, 2021, 102005.
- [54] A.F. Dashti, N.A. S. Salman, R. Adnan, M.A. Zahed, Palm oil mill effluent treatment using combination of low cost chickpea coagulant and granular activated carbon: Optimization via response surface methodology, *Groundwater for Sustainable Development*, Volume 16, 2022, 100709.
- [55] ElSayed, E.E. Natural diatomite as an effective adsorbent for heavy metals in water and wastewater treatment (a batch study), *Water Sci* **2018**, 32, 32-43.
- [56] Du, Y.; Zhen, S.; Wang, J.; Ma, Y.; Wu, J.; Dai, H. FeOOH-MnO<sub>2</sub>/Sepiolite and Fe<sub>2</sub>O<sub>3</sub>-MnO<sub>2</sub>/Diatomite: Highly efficient adsorbents for the removal of As(V), *Appl Clay Sci* **2022**, 222, 106491.
- [57] Shen, T.; Xu, H.; Miao, Y.; Ma, L.; Chen, N.C.; Xie, Q.L. Study on the adsorption process of Cd(II) by Mn-diatomite modified adsorbent, *Mater* **2021**, 300, 130087.
- [58] Wang, J.; Zhang, G.; Qiao, S.; Zhou, J. Magnetic FeO/iron oxide-coated diatomite as a highly efficient adsorbent for recovering phosphorus from water, *Chemical Engineering Journal* **2021**, 412, 128696.
- [59] Song, X.; Li, C.; Chai, Z.; Zhu, Y.; Yang, Y.; Chen, M.; Ma, R.; Liang, X. Wu, J.; Application of diatomite for gallic acid removal from molasses wastewater, *Sci. Total Environ* **2021**, 765, 142711.
- [60] Sofronov, D.; Rucki, M.; Varchenko, V.; Bryleva, E.; Mateychenko, P.; Lebedynskiy, A.; Removal of europium, cobalt and strontium from water solutions using MnO(OH)-modified diatomite, *J. Environ. Chem. Eng* **2022**, 10, 106944.
- [61] Zhao, S.; Huang, G.; Fu, H.; Wang, Y. Enhanced Coagulation/Flocculation by Combining Diatomite with Synthetic Polymers for Oily Wastewater Treatment, *Sep Sci Technol* **2014**, 49, 999-1007.
- [62] Wu, C.-D., Xu, X.-J., Liang, J.-L., Wang, Q., Dong, Q., Liang, W.-L. Enhanced coagulation for treating slightly polluted algae-containing surface water combining polyaluminum chloride (PAC) with diatomite. *Desalination* **2011**, 279, 140–145.
- [63] Jiang, C.; Ding, W.; Zhu, W. Diatomite-enhanced coagulation for algal removal in polluted raw water: performance optimization and pilot-scale study. *Environ Sci Pollut Res* **2021**, 28, 50204–50216.
- [64] Hu, W.; Wu, C. Enhanced coagulation for improving coagulation performance and reducing residual aluminum combining polyaluminum chloride with diatomite. *Environ Sci Pollut Res Int* **2016**, 23, 498-503.
- [65] Cheng, L.; Bi, X.; Liu, C.; X. You, X.; Zhu, W. Effect of Enhanced Coagulation with Diatomite on the Treatment of Oilfield Produced Water. *Proceedings of the 3rd International Conference on Bioinformatics and Biomedical Engineering* **2009**, 1-4.
- [66] Wang, W.H., Li, L.Y., Zhang, X.Q., Qiu, J.Q., Wang, J., Zhang, Y.S. Enhanced Coagulation for Slightly Polluted Seawater Using Ferric Sulfate and Modified Diatomite. *Advanced Materials Research* **2014**, 955–959, 102–107.